Bioconjugate Chemistry

Article

pubs.acs.org/bc

Detection and Imaging of Aggressive Cancer Cells Using an Epidermal Growth Factor Receptor (EGFR)-Targeted Filamentous Plant Virus-Based Nanoparticle

Paul L. Chariou,[†] Karin L. Lee,[†] Amy M. Wen,[†] Neetu M. Gulati,[‡] Phoebe L. Stewart,[‡] and Nicole F. Steinmetz*[,†,§,∥,⊥]

[†]Departments of Biomedical Engineering, [‡]Pharmacology, [§]Radiology, [∥]Materials Science and Engineering, and [⊥]Macromolecular Science and Engineering, Case Western Reserve University Schools of Medicine and Engineering, Cleveland, Ohio 44106, United States

Supporting Information

ABSTRACT: Molecular imaging approaches and targeted drug delivery hold promise for earlier detection of diseases and treatment with higher efficacy while reducing side effects, therefore increasing survival rates and quality of life. Virus-based nanoparticles are a promising platform because their scaffold can be manipulated both genetically and chemically to simultaneously display targeting ligands while carrying payloads for diagnosis or therapeutic intervention. Here, we displayed a 12-amino-acid peptide ligand, GE11 (YHWYGYTPQNVI), on nanoscale filaments formed by the plant virus potato virus X (PVX). Bioconjugation was used to produce fluorescently labeled PVX-GE11 filaments targeted toward the epidermal growth factor receptor (EGFR). Cell detection and imaging was demonstrated using human skin epidermoid carcinoma, colorectal adenocarcinoma, and triple negative breast cancer cell lines (A-431, HT-29, MDA-MB-231), all of which upregulate EGFR to various degrees. Nonspecific uptake in ductal breast carcinoma (BT-474) cells was not observed. Furthermore, co-culture experiments with EGFR$^+$ cancer cells and macrophages indicate successful targeting and partitioning toward the cancer cells. This study lays a foundation for the development of EGFR-targeted filaments delivering contrast agents for imaging and diagnosis, and/or toxic payloads for targeted drug delivery.

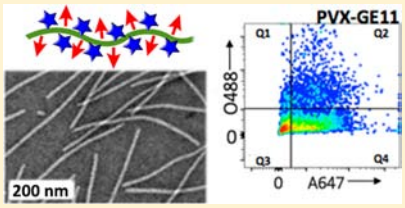

INTRODUCTION

According to the National Cancer Institute, 13.7 million Americans are currently diagnosed with cancer and 600 000 of them are expected to die this year. Only 68% of patients diagnosed are expected to survive more than 5 years due to poor prognosis and the lack of treatment options. Molecular imaging approaches and targeted drug delivery hold promise for earlier detection of disease and treatment with higher efficacy while reducing side effects, therefore increasing survival rates and quality of life. Of particular interest are nanoscale platform technologies that can be functionalized with multiple functional entities, such as toxic payloads (e.g., chemotherapies) and contrast agents (for MRI, PET, etc.), while displaying receptor-specific targeting ligands. Advantages arise from theranostic approaches, where a contrast agent-loaded nanoparticle is used to image the disease site, to test for expression profiles and whether the patient qualifies for a particular treatment approach. If the patient tests positive, treatment can begin with nanoparticles loaded with toxic payloads, therefore providing a route toward personalized nanoparticle interventions.[1,2]

Nanomedicine has led to the development of nanocarriers with prolonged systemic circulation that protect the payload and lead to enhanced accumulation in solid tumors based on the enhanced permeability and retention (EPR) effect.[3,4] Doxil (a liposomal formulation of doxorubicin) and Abraxane (an albumin nanoparticle formulation carrying paclitaxel) increase efficacy of their payloads based on the pathophysiological properties of the target tissue. While passive drug targeting enables tissue accumulation of the carrier and its cargo, cell targeting, entry, and killing may not be achieved. Inefficient cell targeting may promote the development of drug resistance,[5−7] which can lead to recurrence of cancer in a more aggressive form. To overcome this barrier, receptor-targeted nanoparticle formulations are being developed.[8,9]

The tyrosine kinase epidermal growth factor receptor (EGFR) is overexpressed on a variety of human malignancies and is considered an important molecular cancer biomarker.[10] EGFR is a 170 kDa transmembrane glycoprotein member of the ErbB family. Upon activation by endogenous ligands of the EGF family, EGFR is internalized mostly via the clathrin-mediated pathway, triggering cell proliferation, cell division, inhibition of apoptosis, and angiogenesis, implicating EGFR in cancer proliferation and growth.[11−14] Several EGFR-targeting strategies are currently under investigation. Both EGF protein and EGFR antibodies have been used to probe EGFR in tumors; however, limitations to these targeting strategies have been identified, leading to varying degrees of success. Full-

Received: November 24, 2014
Revised: January 21, 2015
Published: January 22, 2015

DOI: 10.1021/bc500545z
Bioconjugate Chem. 2015, 26, 262−269

Scheme 1. Bioconjugation of PVX with NHS-A647 and SM(PEG)$_4$ Linkers, and Subsequent Reaction with GE11 Peptide Yielding a Fluorescent, EGFR-Targeted Nanofilament

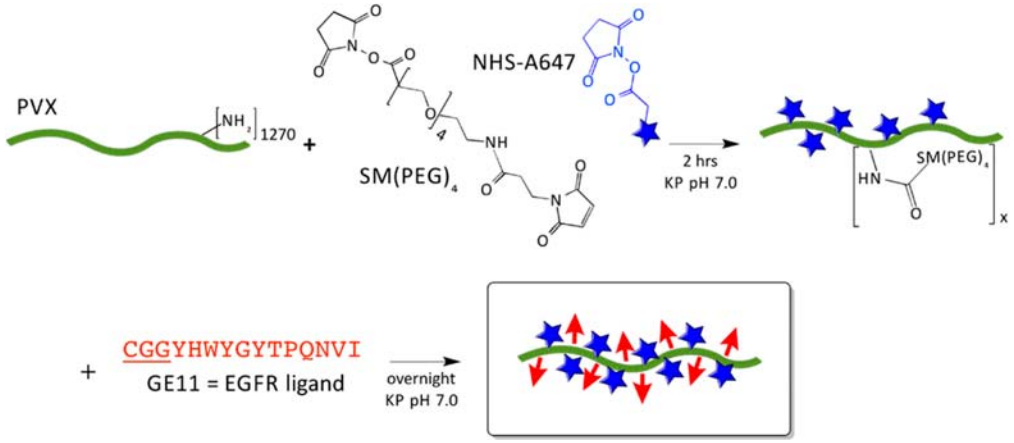

length EGF has a high affinity for EGFR (K_d = 2 nM), but induces cell proliferation,[15,16] an undesirable effect when targeting cancers. Antibody therapy (e.g., Cetuximab) is promising because it blocks activation of the receptor-associated kinases, inhibits cell growth, and induces apoptosis. It has been approved by the FDA for the treatment of head and neck cancer and is under investigation for the treatment of colorectal and breast cancer.[17−20] Nevertheless, recent research has shown that cancer cell resistance to Cetuximab can be mediated via signaling through the HER2/neu protein.[21] The use of peptide ligands conjugated to functionalized nanoparticles carrying contrast agents, toxic payloads, or combinations thereof is particularly promising.[22−25] The GE11 peptide (YHWYGYTPQNVI), discovered through a phage display peptide library screen, binds EGFR with high selectivity and affinity (K_d = 22 nM) and does not activate EGFR-mediated signaling, making it a promising candidate for EGFR-targeted therapies.[26]

In this work, we describe the development of an EGFR-targeted filamentous platform technology using potato virus X (PVX) as a template. PVX is a proteinaceous nanoparticle measuring 515 × 13 nm^2; it is composed of 1270 identical coat proteins, each of which can be modified at a solvent-exposed lysine residue using *N*-hydroxysuccinimide activated probes.[27] We recently demonstrated that the high aspect ratio and elongated shape of PVX increased passive tumor homing in a variety of models, including human tumor xenografts of breast cancer, fibrosarcoma, squamous sarcoma, brain cancer, and colon cancer. Furthermore, tissue penetration of filamentous platforms is enhanced in comparison to spherical counterparts.[27] These properties make PVX a promising platform for nanomedical research and technology development. In addition to its shape, PVX, as well as other plant virus-based nanomaterials, offers further benefits compared to synthetic counterparts. Virus-based nanoparticles (VNPs) are genetically encoded, programmed to self-assemble into monodisperse and highly symmetrical biomaterials. Because these materials are genetically encoded, high-aspect-ratio materials can be obtained with spatial control at the atomic level and with impeccable reproducibility, a level of control not yet achievable with synthetic chemistry. VNPs are biocompatible and biodegradable, and do not cause acute toxicity in vitro or in vivo.[28] Plant-based VNPs can be produced in plants in high yields at a relatively low cost through molecular farming in plants, thus providing a realistic platform for translation and commercialization.

We describe the synthesis and application of GE11-modified PVX filaments for molecularly targeted detection and imaging of EGFR$^+$ cancer cells. Target-specificity of PVX-GE11 was evaluated using the EGFR-positive human skin epidermoid carcinoma (A-431), colorectal adenocarcinoma (HT-29), and triple negative breast cancer (MDA-MB-231) cell lines, as well as the EGFR-negative ductal breast carcinoma (BT-474) cell line. Furthermore, target-specificity was evaluated in co-culture experiments with cancer cells and macrophages.

RESULTS AND DISCUSSION

Bioconjugation of Targeting and Imaging Moieties. PVX was produced through farming in *N. benthamiana* plants using previously established protocols[29] and extracted at yields of 20 mg of pure PVX from 100 g of infected leaf material. GE11 peptide was synthesized with an amino-terminal cysteine residue with intervening GG spacer for bioconjugation (CGGYHWYGYTPQNVI). Fluorescently labeled, EGFR-targeted PVX filaments were obtained using a two-step bioconjugation reaction (Scheme 1). Briefly, a bifunctional PEG linker with a 24.6 Å spacer arm (SM(PEG)$_4$) and Alexa Fluor 647 succinimidyl ester (NHS-A647) were conjugated to solvent-exposed lysines on PVX followed by addition of the cysteine-terminated GE11 peptide targeting the maleimide side groups of SM(PEG)$_4$. Nontargeted particles were also synthesized by omitting the second step in order to assess nonspecific cell binding. The PVX-based formulations were subsequently characterized by UV/visible spectroscopy, denaturing gel electrophoresis (SDS-PAGE), and transmission electron microscopy (TEM) to quantify the degree of modification and confirm structural integrity (Figure 1).

UV/visible spectroscopy and SDS-PAGE were used to quantify the degree of labeling with A647 fluorophore and GE11 peptide. Based on the Beer−Lambert law and fluorophore- and PVX-specific extinction coefficients, it was determined that approximately 300 dyes per PVX were displayed (Figure 1). Because dyes were conjugated in the first reaction step prior to separation of the samples for further modification, the targeted and nontargeted control samples (A647-PVX-GE11 and A647-PVX) displayed the same number of fluorophores. (It should be noted that the GE11 peptide contributes to the absorbance at 280 nm (Figure 1A), and

DOI: 10.1021/bc500545z
Bioconjugate Chem. 2015, 26, 262−269

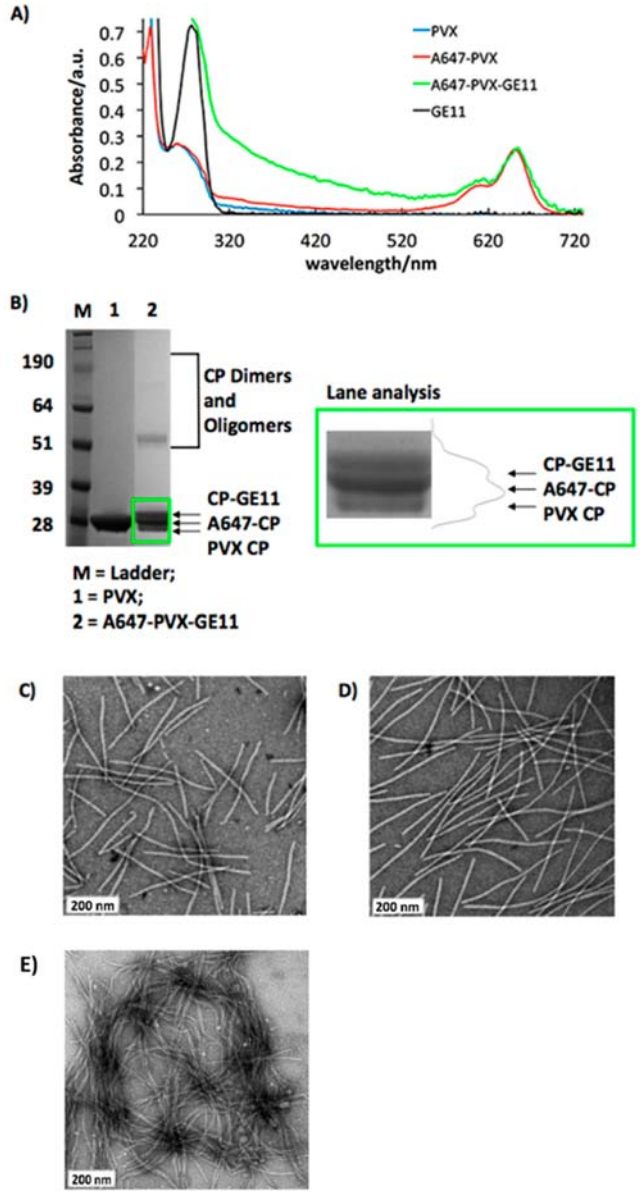

Figure 1. Characterization of A647-PVX-GE11 particles. (A) UV/visible spectra of native and modified PVX nanoparticles and GE11 peptide. (B) Particles after electrophoretic separation on 4−12% SDS-PAGE gel run in MOPS buffer visualized with white light after Coomassie staining. M = SeeBlue Plus2 molecular weight standard; the molecular weight in kDa is indicated on the left. 1 = PVX, 2 = A647-PVX-GE11; inset shows lane analysis performed using *ImageJ* software. TEM images of negatively stained (C) A647-PVX and (D) A647-PVX-GE11. (E) TEM image of negatively stained PVX after 1 h incubation in serum.

therefore, A647 loading was quantified prior to conjugation of GE11).

SDS-PAGE further confirmed covalent attachment of the A647 fluorophores and GE11 peptides, as indicated by higher-molecular-weight bands (Figure 1B). The PVX coat protein (CP) has a molecular weight of 25 kDa; higher molecular weights indicate the addition of A647 (~1.3 kDa) and GE11 (~1.7 kDa). Band analysis and *ImageJ* were used to quantify the degree of labeling, and data indicate a ratio of CP:A647-CP:A647-CP-GE11 of 1:2:2, indicating that 40% (or 500) of the coat proteins are modified with A647 and 40% of the proteins display GE11 targeting. PVX consists of 1270 identical copies of a CP, each with a single reactive lysine side chain;[30] dual labeling is therefore not expected. There is some discrepancy between the SDS-PAGE analysis and UV/visible spectroscopy quantification of the fluorophore: SDS gels indicate 500 dyes per PVX while UV/visible data indicate 300 dyes per PVX—the difference is likely explained by the A647 contributing to the staining (the bands are visible under white light without Coomassie Blue staining, not shown), therefore enhancing the band intensity. Gel electrophoresis indicates the presence of dimers and oligomers; these multimeric coat proteins are typically observed in SDS-PAGE after PVX conjugation with peptides using the $SM(PEG)_4$ linker.[31] This may indicate that a small number of coat proteins are interlinked through the bifunctional $SM(PEG)_4$ linker (targeting lysine and potentially cysteine residues). Nonetheless, it is important to note that interparticle cross-linking was not observed in TEM images (Figure 1C,D), so any potential cross-linking is likely between coat proteins of the same particle. TEM imaging confirmed that the particles remained structurally intact after two rounds of chemical modification (Figure 1C,D). In addition, we confirmed PVX stability in serum (Figure 1E).

Cell Binding Experiments. To test the affinity of fluorescent-labeled, EGFR-targeted PVX particles for cells expressing EGFR, we conducted a series of flow cytometry experiments using a panel of cancer cell lines that upregulate EGFR to various degrees (Figure 2): human skin epidermoid carcinoma, colorectal adenocarcinoma, and triple negative breast cancer cell lines (A-431, HT-29, MDA-MB-231).[32−36] The $EGFR^-$ ductal breast carcinoma (BT-474) cell line was used to assess nonspecific uptake.[34]

An anti-EGFR FITC-labeled antibody and flow cytometry were used to confirm the level of EGFR expression on the cell lines tested (Figure 2A,C). In agreement with the literature,[32−36] MDA-MB-231, HT-29, and A-431 cells tested positive for EGFR (with HT-29 and A-431 cells expressing higher levels of EGFR compared to MDA-MB-231 cells) and BT-474 cells were EGFR-negative.

Next, the cell target-specificity of the A647-PVX-GE11 formulation was evaluated using flow cytometry (Figure 2B,C). In $EGFR^+_{high}$ cells, HT-29 and A-431, targeting of the EGFR-specific A647-PVX-GE11 probe was significantly increased compared to nonspecific PVX−cell interactions. Nonspecific cell interactions have been previously reported for PVX,[29] and are frequently observed for synthetic nanoparticle formulations as well.[37] Overall, cell targeting efficiency of the A647-PVX-GE11 probe followed a trend, i.e., A647-PVX-GE11 was highest in $EGFR^+_{high}$ cells (HT-29 and A-431), while moderate and negligible uptake was observed in $EGFR^+_{low}$ cells (MDA-MB-231) and $EGFR^-$ cells (BT-474), respectively.

Nonspecific cell uptake of nontargeted PVX was significantly lower in the breast cancer cells lines versus the epidermoid carcinoma and colorectal adenocarcinoma cells; this may be explained by different metabolic rates of these cell types. There was no difference in cell uptake comparing the targeted A647-PVX-GE11 versus the nontargeted A647-PVX formulation using the $EGFR^-$ BT-474 cell line, indicating that the targeting ligand confers specificity toward EGFR and does not increase nonspecific cell uptake. Using $EGFR^+_{low}$ cells, MDA-MB-231, we found that, while A647-PVX-GE11 showed increased cell uptake versus A647-PVX, statistical significance was not

DOI: 10.1021/bc500545z
Bioconjugate Chem. 2015, 26, 262−269

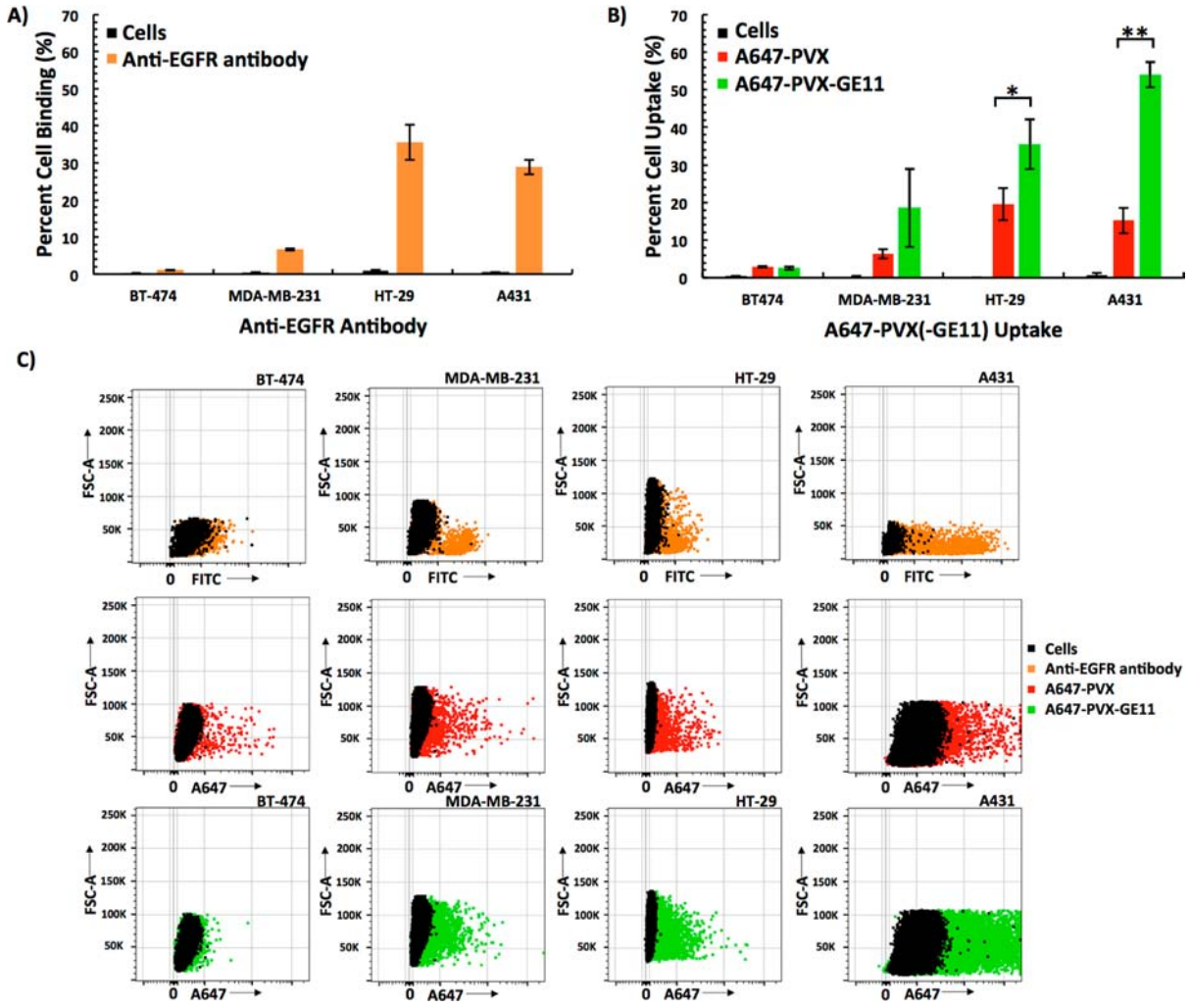

Figure 2. Flow cytometry quantification of EGFR expression using (A) an EGFR-specific antibody and (B) quantification of PVX−cell interactions comparing an EGFR-targeted A647-PVX-GE11 and nontargeted A647-PVX formulation. All samples were measured in triplicates and analyzed using *FlowJo* software. Error bars indicate the standard deviation (* $p < 0.05$ and ** $p < 0.01$). (C) Representative dot plots showing the fluorescence overlay of unstained cells (black) with cells incubated with either FITC-labeled EGFR antibody (orange), A647-PVX (red), or A647-PVX-GE11 (green).

reached, which may reflect the relatively low EGFR expression level.

Next, we set out to determine cell-specificity in co-culture experiments with cancer cells and macrophages. Understanding the partitioning coefficient of a nanoparticle between the target cancer cell and nontarget macrophage populations is important, because mononuclear phagocytic clearance remains a challenge for successful translation of nanomedicines. Cell mixtures using 20:80 RAW264.7:HT-29 cells were incubated with either A647-PVX or A647-PVX-GE11 and cell interactions were quantified using flow cytometry (Figure 3). RAW264.7 cells were differentiated from HT-29 cells through staining of CD11b surface markers (Figure 3A, gates Q1 + 2). As expected, nontargeted and targeted PVX formulations were taken up by macrophages, but uptake in macrophages is not enhanced upon conjugation of the GE11 targeting ligand (Figure 3). 27% and 35% of macrophages scored positive for A647-PVX and A647-PVX-GE11, respectively, with no statistically significant differences between the two populations, indicating that the addition of a targeting ligand does not increase nonspecific uptake into macrophages.

For the nontargeted A647-PVX formulation, macrophage interactions are enhanced compared to nonspecific HT-29−PVX interactions (RAW264.7 > HT-29 with $p < 0.05$), which may be explained by the different modes of uptake: macrophages interact with nanomaterials via phagocytosis and cancer cells via endocytosis.[38] This partitioning between macrophages and cancer cells was reversed when the targeted A647-PVX-GE11 formulation was considered: here, partitioning favored cancer cells. A significantly larger proportion of HT-29 cells (78%) interacted with the A647-PVX-GE11 particles compared to macrophages (HT-29 ≫ RAW264.7 with $p < 0.0005$); binding to macrophages remained low (35%) and at comparable levels as observed using the nontargeted A647-PVX formulation (27%).

CONCLUSION

Overall, the data support that A647-PVX-GE11 targets EGFR$^+$ cells. We have previously shown that fluorescently labeled PVX is taken up by different cell types.[30] These nonspecific cell interactions may be explained by PVX's positive surface charge leading to electrostatic attractions with the negatively charged cell membrane; we also showed that this can be overcome

DOI: 10.1021/bc500545z
Bioconjugate Chem. 2015, 26, 262−269

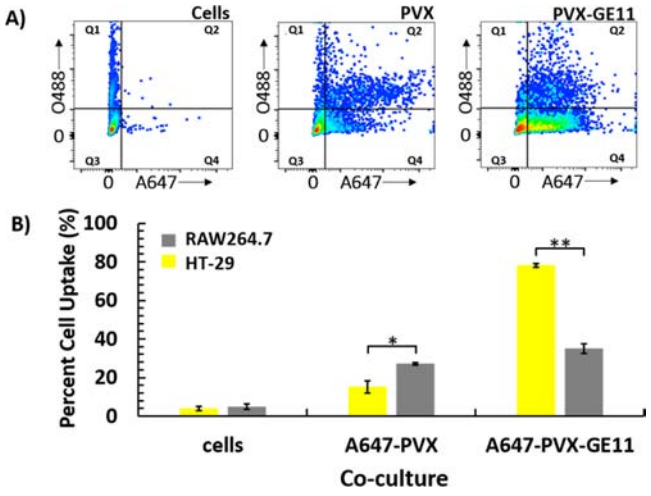

Figure 3. (A) Representative dot plots of co-cultured RAW264.7 macrophages and HT-29 cancer cells at a 20:80 ratio. Macrophages were differentiated from HT-29 cells using CD11b staining (Oregon Green 488 channel); PVX was detected based on the A647 label (A647 channel). Q1 = RAW264.7 cells (CD11b positive) that are PVX-negative; Q2 = RAW264.7 cells (CD11b positive) positive for A647-PVX(-GE11); Q3 = HT-29 cells (CD11b negative) that are PVX-negative; Q4 = HT-29 cells (CD11b negative) positive for A647-PVX(-GE11). (B) Percent cell uptake distribution of A647-PVX and A647-PVX-GE11 comparing HT-29− and RAW264.7−PVX interactions. All samples were measured in triplicate and analyzed using *FlowJo* software, with error bars indicating the standard deviation (* $p < 0.05$ and ** $p < 0.0005$).

through PEGylation.[27] While we did not employ PEG coatings in this study, our data indicate that display of EGFR-targeting ligand GE11 enables targeting of EGFR$^+$ cancer cells, while not increasing nonspecific cell interactions with EGFR$^-$ cancer cells or macrophages.

EGFR-targeted contrast agents and therapeutic formulations are under development; however, all are spherical and this may not be optimal. Mounting evidence suggests advantageous behavior of elongated, filamentous nanomaterials for nanomedical applications. Elongated filaments exhibit increased margination toward the vessel wall, therefore increasing EPR tumor homing and molecular targeting.[39−41] Molecular target recognition is further enhanced because elongated materials present ligands more effectively to the flat vessel wall or target cells compared to their spherical counterparts.[42,43] Finally, data indicate that elongated materials have increased immune evasion and reduced macrophage uptake, therefore further contributing to synergistic target enhancement.[44] Therefore, we turned toward the development of an EGFR-targeted filament using the PVX platform technology. This is the first example of a receptor-targeted PVX-based optical imaging agent. While we demonstrate optical detection of EGFR$^+$ cancer cells here, fluorescent dyes could be exchanged with contrast agents used in clinical imaging, including Gd(DOTA) for magnetic resonance imaging[45] or ^{64}Cu for position emission spectroscopy.[46] Alternatively, toxic payloads such as chemotherapeutic, peptide, or protein drugs could be incorporated to aid therapeutic intervention.[47]

Our data are in good agreement with reports using synthetic nanomaterials targeted toward EGFR. For example, poly(inosine/cytosine) GE11 polyplex formulations show promise in nonviral gene therapy targeting EGFR$^+$ disease.[48] Similarly, GE11-targeted liposomes have been developed to target EGFR expressing cells.[49,50] EGFR-targeted virus-based materials have also been developed and studied; examples include the 30-nm-sized icosahedrons formed by bacteriophage Qβ. Qβ was genetically engineered to express EGF protein in low copy number as a coat protein fusion; the Qβ-EGF chimera was shown to target EGFR$^+$ cells and promotes autophosphorylation of the EGF receptor, leading to apoptosis of A-431 cells (a phenomenon specific to A-431 cells).[51] A different approach used an EGFR-retargeted measles virus (EGFR-MV) strain engineered with a single chain antibody specific for EGFR for targeted oncolytic viral therapy.[52] We expect presentation of an EGFR-specific targeting peptide on a filamentous particle will exhibit advantageous behavior in vivo.

In summary, this report details the synthesis of fluorescently labeled, EGFR-targeted filamentous nanoparticles using the PVX platform technology and bioconjugate chemistry. The proteinaceous particles remained stable after two rounds of bioconjugation, and several hundred copies of fluorophores (~300/PVX) and EGFR-specific GE11 peptide ligands (~500/PVX) were incorporated. Serum stability was confirmed, and cell target specificity was demonstrated using a panel of EGFR$^+$ and EGFR$^-$ cancer cells and macrophages. We demonstrate target-specificity and preferred partitioning to cancer cells versus macrophages using the targeted A647-PVX-GE11 formulation. These results offer a critical step toward the development of a scalable nanoparticle platform technology for imaging and/or treatment of EGFR-expressing cancers. Nevertheless, the road toward translation of this technology must be paved by detailed in vivo studies evaluating both the efficacy as well as potential adverse effects.

MATERIALS AND METHODS

PVX Propagation and Purification. *Nicotiana benthamiana* plants were seeded and grown for 4−6 weeks in humidity controlled growth chambers (15 h day cycle: 25 °C and 65% rel. humidity; night cycle: 23 °C and 70% rel. humidity). Infection was induced through mechanical inoculation using 150 ng μL^{-1} purified PVX in 0.1 M potassium phosphate (KP) buffer pH 7.0; leaves were dusted with carborundum (Alfa Aesar). Plants were propagated for 21−25 days post inoculation and purified using established protocols.[27] Purified PVX particles were stored in KP buffer; concentration and purity was determined using UV/visible spectroscopy, and PVX particle integrity was determined by transmission electron microscopy (see below).

PVX Bioconjugation. GE11 peptide was obtained from the Cleveland Clinic Molecular Biotechnology Core Facility. GE11 peptide was synthesized with an amino-terminal cysteine residue with intervening GG spacer (CGGYHWYGYTPQNVI). Fluorescently labeled, EGFR-targeted PVX were synthesized using a two-step reaction: first, succinimidyl-[(*N*-maleimidopropionamido)-tetraethylene glycol] ester (SM-(PEG)$_4$, Pierce) and Alexa Fluor 647 succinimdyl ester (A647-NHS, Life Technologies) in DMSO were added at a 2-fold molar excess per PVX coat protein to give a final of 10% (v/v) DMSO in KP buffer. After 2 h incubation at room temperature, excess linker and fluorescent molecules were removed using either 10 kDa molecular weight cutoff centrifugal filters (Millipore) or ultracentrifugation (42 000 rpm using 50.2 Ti fixed angle rotor for 3 h over a 40% (w/v) sucrose cushion), prior to immediately proceeding to the second step. GE11 targeting ligand was added using a 20-fold molar excess per PVX coat protein; the reaction was carried out

DOI: 10.1021/bc500545z
Bioconjugate Chem. 2015, 26, 262−269

overnight in 10% (v/v) DMSO in KP buffer. Controls were also obtained by omitting the addition of the targeting ligand. Samples were purified by ultracentrifugation over a 40% (w/v) sucrose cushion (42 000 rpm using 50.2 Ti fixed angle rotor for 3 h). Pellets were resuspended in KP buffer and stored in the dark at 4 °C until further processing.

UV/visible Spectroscopy. A NanoDrop Spectrophotometer (Thermo Scientific) was used to measure the UV/visible spectra of native and modified PVX nanoparticles. The amount of A647 fluorophore per PVX was determined based on the ratio of dye:PVX concentration, making use of the Beer–Lambert law and dye- and PVX-specific extinction coefficients: PVX: ε(260 nm) = 2.97 mL mg^{-1} cm^{-1}, molecular weight of PVX = 35 × 10^6 g mol^{-1}; A647: ε(651 nm) = 270 000 M^{-1} cm^{-1}, molecular weight of A647 = 1300 g mol^{-1}.

Denaturing Gel Electrophoresis. 15 μg of PVX control, A647 PVX-PEG, and A647 PVX-PEG-GE11 were denatured (100 °C for 5 min) in 1× LDS loading dye (Life Technologies) to obtain a final volume of 20 μL. PVX proteins, as well as SeeBlue Plus2 ladder (Life Technologies), were separated for 40 min at 200 V and 120 mA using a 4–12% NuPage precast gel in 1× MOPS buffer (Life Technologies). Gels were photographed before and after staining with Coomassie Blue (0.25% w/v) using the AlphaImager (Biosciences) imaging system under white light.

Transmission Electron Microscopy. Drops of PVX particles (20 μL, 0.1 mg mL^{-1}) were added to Formvar carbon film coated copper TEM grids (Electron Microscopy Sciences) for 5 min at room temperature. The grids were washed with deionized water and stained with 2% (w/v) uranyl acetate in deionized water for another 5 min. A Zeiss Libra 200FE transmission electron microscope was used to inspect samples at 200 kV, or a FEI Tecnai G$_2$ Spirit transmission electron microscope at 120 kV.

Particle Stability in Serum. PVX particles were incubated in FBS at a concentration of 50 μg/mL for 1 h at 37 °C. PVX particles were then purified over a 30% (w/v) sucrose gradient using ultracentrifugation (42 000 rpm using 50.2 Ti fixed angle rotor for 3 h), prior to TEM imaging.

Tissue Culture. *1. Cell Maintenance.* All cell lines were obtained from ATCC. All culture media reagents were purchased from Invitrogen, unless indicated otherwise. MDA-MB-231 cells (triple negative breast cancer) were cultured in RPMI-1640 medium with L-glutamine (Fisher). HT-29 cells (colon cancer) were maintained in McCoy's 5A medium with L-glutamine. A-431 cells (epidermal carcinoma) and RAW264.7 cells (murine macrophage) were cultured in high glucose Dulbecco's modified Eagle medium (DMEM) with L-glutamine. BT-474 cells (breast cancer) were maintained in Hybri-Care Medium (ATCC). For all cell lines, media were supplemented with 10% (v/v) FBS and 1% (v/v) penicillin–streptomycin. BT-474 cells were additionally supplemented with 1.5 g L^{-1} sodium bicarbonate. Cells were grown at 37 °C and 5% CO$_2$.

2. Flow Cytometry. EGFR Staining. MDA-MB-231, HT-29, A-431, and BT-474 cells were grown to confluency and collected using an enzyme-free Hank's based cell dissociation buffer (Invitrogen). Cells (500 000 cells/200 μL media/well) were added to untreated 96-well v-bottom plates (VWR). EGFR was stained using an anti-EGFR FITC-labeled antibody (Millipore, 1.25 dilution as per manufacturer's recommendation) and cells were incubated at 37 °C, 5% CO$_2$ for 60 min. After incubation, cells were spun down at 500 *g* for 4 min, supernatant was removed, and cells were washed twice in FACS buffer (0.1 mL 0.5 M EDTA, 0.5 mL FBS, and 1.25 mL 1 M HEPES pH 7.0 in Ca^{2+} and Mg^{2+} free PBS (50 mL total volume)). Cells were fixed in 2% (v/v) paraformaldehyde in FACS buffer at room temperature for 10 min and washed twice and resuspended using FACS buffer. All samples were prepared in triplicate. The BD LSR II flow cytometer was used to analyze samples and 10 000 gated events were recorded. Data were analyzed using *FlowJo 8.6.3* software (http://www.flowjo.com/).

EGFR-Targeting Using PVX-Based Filaments. MDA-MB-231, HT-29, A-431, and BT-474 cells were grown to confluency and collected using enzyme-free Hank's-based cell dissociation buffer. Cells (500 000 cells/200 μL media/well) were added to untreated 96-well v-bottom plates. Triplicates of no particles, A647 PVX-PEG, and A647 PVX-PEG-GE11 were added at a concentration of 100 000 particles/cell and incubated for 2 h at 37 °C, 5% CO$_2$. Following incubation, cells were spun down at 500 *g* for 4 min and supernatant was removed. Cells were then washed twice in FACS buffer and fixed in 2% (v/v) paraformaldehyde in FACS buffer at room temperature for 10 min. Cells were washed twice after fixing and resuspended in FACS buffer. FACS and data analysis were carried out as described above.

Cell Co-Culture. HT-29 and RAW264.7 cells were grown to confluency and collected using an enzyme-free Hank's based cell dissociation buffer. Cell mixtures containing 20:80 ratio of RAW264.7:HT-29 cell were evaluated. Cells were prepared as described above and PVX-based formulations were added at 100 000 particles/cell as described above and incubated for 2 h at 37 °C, 5% CO$_2$. Following incubation, cells were spun down at 500 *g* for 4 min and supernatant was removed. Cells were then washed twice in FACS buffer. RAW264.7 cells were differentiated from HT-29 cells through staining of CD11b surface markers. Cells were blocked with rat anti-mouse CD16/CD32 (Fc Block) (BD Biosciences) as follows: a working solution Fc Block was made using 1 μL Fc Block/200 μL FACS buffer. 100 μL of the working solution was added to each well and incubated for 30 min on ice. Following incubation, cells were washed then stained using 1 μL anti-mouse CD11b (BD Biosciences) in 100 μL FACS buffer per well and incubated for 30 min on ice. Cells were washed once and fixed as described previously. FACS and data analysis were carried out as described above.

■ ASSOCIATED CONTENT

Supporting Information

Additional confocal microscopy methods and data. This material is available free of charge via the Internet at http://pubs.acs.org.

■ AUTHOR INFORMATION

Corresponding Author

*E-mail: nicole.steinmetz@case.edu.

Author Contributions

Paul L. Chariou and Karin L. Lee contributed equally.

Notes

The authors declare no competing financial interest.

■ ACKNOWLEDGMENTS

This work was supported by a grant from the National Science Foundation (NSF): CMMI NM 1333651, Mt. Sinai Foundation and Case Western Reserve University start-up

DOI: 10.1021/bc500545z
Bioconjugate Chem. 2015, 26, 262–269

funds to N.F.S. K.L.L. acknowledges the National Institutes of Health (NIH) NCI R25 CA148052 Cancer Pharmacology training grant. N.M.G. acknowledges the NIH T32 GM008803 Molecular Therapeutics training grant. A.M.W. acknowledges the NIH T32 HL105338 Cardiovascular Research training grant.

REFERENCES

(1) Lammers, T., Kiessling, F., Hennink, W. E., and Storm, G. (2012) Drug targeting to tumors: Principles, pitfalls and (pre-) clinical progress. *J. Controlled Release 161*, 175−187.
(2) Portney, N. G., and Ozkan, M. (2006) Nano-oncology: drug delivery, imaging, and sensing. *Anal. Bioanal. Chem. 384*, 620−30.
(3) Matsumura, Y., Maeda, H., and Smancs, A. (1986) A new concept for macromolecular therapeutics in cancer chemotherapy: mechanism of tumoritropic accumulation of proteins and the antitumor agent smancs a new concept for macromolecular therapeutics in cancer chemotherapy: mechanism of tumoritropic accum. *Cancer Res. 46*, 6387−6392.
(4) Maeda, H. (2001) The enhanced permeability and retention (EPR) effect in tumor vasculature: the key role of tumor-selective macromolecular drug targeting. *Adv. Enzyme Regul. 41*, 189−207.
(5) Moitra, K., Lou, H., and Dean, M. (2011) Multidrug efflux pumps and cancer stem cells: insights into multidrug resistance and therapeutic development. *Clin. Pharmacol. Ther. 89*, 491−502.
(6) Fletcher, J. I., Haber, M., Henderson, M. J., and Norris, M. D. (2010) ABC transporters in cancer: more than just drug efflux pumps. *Nat. Rev. Cancer 10*, 147−56.
(7) Cho, K., Wang, X., Nie, S., Chen, Z. G., and Shin, D. M. (2008) Therapeutic nanoparticles for drug delivery in cancer. *Clin. Cancer Res. 14*, 1310−6.
(8) Bareford, L. M., and Swaan, P. W. (2007) Endocytic mechanisms for targeted drug delivery. *Adv. Drug Delivery Rev. 59*, 748−58.
(9) Danhier, F., Feron, O., and Préat, V. (2010) To exploit the tumor microenvironment: Passive and active tumor targeting of nanocarriers for anti-cancer drug delivery. *J. Controlled Release 148*, 135−46.
(10) Nicholson, R., Gee, J. M., and Harper, M. (2001) EGFR and cancer prognosis. *Eur. J. Cancer 37*, 9−15.
(11) Mickler, F. M., Mo, L., Ruthardt, N., Ogris, M., and Wagner, E. (2012) Tuning nanoparticle uptake: live-cell imaging reveals two distinct endocytosis mechanisms mediated by natural and artificial EGFR targeting ligand. *Nano Lett. 12*, 3417−3423.
(12) Rocha-lima, C. M., Soares, H. P., Raez, L. E., and Singal, R. (2007) EGFR targeting of solid tumors. *Cancer Control: Journal of the Moffitt Cancer Center 14*, 295−304.
(13) Hackel, P. O., Zwick, E., Prenzel, N., and Ullrich, A. (1999) Epidermal growth factor receptors: critical mediators of multiple receptor pathways. *Curr. Opin. Cell Biol. 11*, 184−189.
(14) Cawley, L. J. M. C., Brien, P. O., and Hudson, L. G. (2014) Overexpression of the epidermal growth factor receptor contributes to enhanced ligand-mediated motility in keratinocyte cell lines. *Endocrinology 138*, 121−127.
(15) Kitai, Y., Fukuda, H., Enomoto, T., Asakawa, Y., Suzuki, T., Inouye, S., and Handa, H. (2011) Cell selective targeting of a simian virus 40 virus-like particle conjugated to epidermal growth factor. *J. Biotechnol. 155*, 251−6.
(16) Kickhoefer, V. A., Han, M., Raval-fernandes, S., Poderycki, M. J., Moniz, R. J., Vaccari, D., Silvestry, M., Stewart, P. L., Kelly, K. A., and Rome, L. H. (2009) Targeting vault nanoparticles to specific cell surface receptors. *ACS Nano 3*, 27−36.
(17) Baselga, J. (2001) The EGFR as a target for anticancer therapy—focus on cetuximab. *Eur. J. Cancer 37*, 16−22.
(18) Liu, B., Fang, M., Schmidt, M., Lu, Y., Mendelsohn, J., and Fan, Z. (2000) Induction of apoptosis and activation of the caspase cascade by anti-EGF receptor monoclonal antibodies in DiFi human colon cancer cells do not involve the c-jun N-terminal kinase activity. *Br. J. Cancer 82*, 1991−1999.
(19) Galizia, G., Lieto, E., De Vita, F., Orditura, M., Castellano, P., Troiani, T., Imperatore, V., and Ciardiello, F. (2007) Cetuximab, a chimeric human mouse anti-epidermal growth factor receptor monoclonal antibody, in the treatment of human colorectal cancer. *Oncogene 26*, 3654−60.
(20) Raff, J. P., Rajdev, L., Malik, U., Novik, Y., Manalo, J. M., Negassa, A., Hopkins, U., Sarta, C., and Sparano, J. a. (2004) Phase II study of weekly docetaxel alone or in combination with trastuzumab in patients with metastatic breast cancer. *Clin. Breast Cancer 4*, 420−427.
(21) Yonesaka, K., Zejnullahu, K., Okamoto, I., Satoh, T., Cappuzzo, F., Souglakos, J., Ercan, D., Rogers, A., Roncalli, M., Takeda, M., et al. (2011) Activation of ERBB2 signaling causes resistance to the EGFR-directed therapeutic antibody cetuximab. *Sci. Transl. Med. 3*, 99ra86.
(22) Press, D. (2012) Cyclic RGD peptide-modified liposomal drug delivery system: enhanced cellular uptake in vitro and improved pharmacokinetics in rats. *Int. J. Nanomedicine 7*, 3803−3811.
(23) Lee, G. Y., Kim, J.-H., Oh, G. T., Lee, B.-H., Kwon, I. C., and Kim, I.-S. (2011) Molecular targeting of atherosclerotic plaques by a stabilin-2-specific peptide ligand. *J. Controlled Release 155*, 211−7.
(24) Song, S., Liu, D., Peng, J., Deng, H., Guo, Y., Xu, L. X., Miller, A. D., and Xu, Y. (2009) Novel peptide ligand directs liposomes toward EGF-R high-expressing cancer cells in vitro and in vivo. *FASEB J. 23*, 1396−404.
(25) Zhang, Y., Zhang, H., Wang, X., Wang, J., Zhang, X., and Zhang, Q. (2012) The eradication of breast cancer and cancer stem cells using octreotide modified paclitaxel active targeting micelles and salinomycin passive targeting micelles. *Biomaterials 33*, 679−91.
(26) Li, Z., Zhao, R., Wu, X., Sun, Y., Yao, M., Li, J., Xu, Y., and Gu, J. (2005) Identification and characterization of a novel peptide ligand of epidermal growth factor receptor for targeted delivery of therapeutics. *FASEB J. 19*, 1978−85.
(27) Shukla, S., Ablack, A. L., Wen, A. M., Lee, K. L., Lewis, J. D., and Steinmetz, N. F. (2013) Increased tumor homing and tissue penetration of the filamentous plant viral nanoparticle Potato virus X. *Mol. Pharmaceutics 10*, 33−42.
(28) Shukla, S., Dickmeis, C., Nagarajan, a. S., Fischer, R., Commandeur, U., and Steinmetz, N. F. (2014) Molecular farming of fluorescent virus-based nanoparticles for optical imaging in plants, human cells and mouse models. *Biomater. Sci. 2*, 784−797.
(29) Lee, K. L., Uhde-Holzem, K., Fisher, R., Commendeur, U., and Steinmetz, N. F. (2014) Genetic engineering and chemical conjugation of potato virus X. *Methods Mol. Biol.*, 3−21.
(30) Steinmetz, N. F., Mertens, M. E., Taurog, R. E., Johnson, J. E., Commandeur, U., Fischer, R., and Manchester, M. (2010) Potato virus X as a novel platform for potential biomedical applications. *Nano Lett. 10*, 305−12.
(31) Shukla, S., Wen, A. M., Commandeur, U., and Steinmetz, N. F. (2014) Presentation of HER2 epitopes using a filamentous plant virus-based vaccination platform. *J. Mater. Chem. B 2*, 6249−6258.
(32) Kawamotos, T., Mendelsohnsq, J., Le, A., Sato, G. H., Lazarlt, C. S., and Gill, G. N. (1984) Relation of epidermal growth factor receptor concentration to growth of human epidermoid carcinoma A431 cells. *J. Biol. Chem. 259*, 7761−7766.
(33) Wiley, H. S. (1988) Anomalous binding of epidermal growth factor to A431 cells is due to the effect of high receptor densities and a saturable endocytic system. *J. Cell Biol. 107*, 801−810.
(34) Rae, J. M., Scheys, J. O., Clark, K. M., Chadwick, R. B., Kiefer, M. C., and Lippman, M. E. (2004) EGFR and EGFRvIII expression in primary breast cancer and cell lines. *Breast Cancer Res. Treat. 87*, 87−95.
(35) Wang, K., Wang, K., Li, W., Huang, T., Li, R., Wang, D., Shen, B., and Chen, X. (2009) Characterizing breast cancer xenograft epidermal growth factor receptor expression by using near-infrared optical imaging. *Acta Radiol. 50*, 1095−103.
(36) Balin-Gauthier, D., Delord, J.-P., Rochaix, P., Mallard, V., Thomas, F., Hennebelle, I., Bugat, R., Canal, P., and Allal, C. (2006) In vivo and in vitro antitumor activity of oxaliplatin in combination with cetuximab in human colorectal tumor cell lines expressing different level of EGFR. *Cancer Chemother. Pharmacol. 57*, 709−18.

DOI: 10.1021/bc500545z
Bioconjugate Chem. 2015, 26, 262−269

(37) Kelf, T. A., Sreenivasan, V. K. A., Sun, J., Kim, E. J., Goldys, E. M., and Zvyagin, A. (2010) Non-specific cellular uptake of surface-functionalized quantum dots. *Nanotechnlogy 21*, 1−14.
(38) Hillaireau, H., and Couvreur, P. (2009) Nanocarriers' entry into the cell: relevance to drug delivery. *Cell. Mol. Life Sci. 66*, 2873−96.
(39) Christian, D. A., Cai, S., Garbuzenko, O. B., Harada, T., Allison, L., Minko, T., and Discher, D. E. (2009) Flexible filaments for in vivo imaging and delivery: persistent circulation of filomicelles opens the dosage window for sustained tumor shrinkage. *Mol. Pharmaceutics 6*, 1343−1352.
(40) Chauhan, V. P., Popović, Z., Chen, O., Cui, J., Fukumura, D., Bawendi, M. G., and Jain, R. K. (2011) Fluorescent nanorods and nanospheres for real-time in vivo probing of nanoparticle shape-dependent tumor penetration. *Angew. Chem., Int. Ed. 50*, 11417−20.
(41) Decuzzi, P., Godin, B., Tanaka, T., Lee, S.-Y., Chiappini, C., Liu, X., and Ferrari, M. (2010) Size and shape effects in the biodistribution of intravascularly injected particles. *J. Controlled Release 141*, 320−7.
(42) Doshi, N., Prabhakarpandian, B., Rea-Ramsey, A., Pant, K., Sundaram, S., and Mitragotri, S. (2010) Flow and adhesion of drug carriers in blood vessels depend on their shape: a study using model synthetic microvascular networks. *J. Controlled Release 146*, 196−200.
(43) Lee, S.-Y., Ferrari, M., and Decuzzi, P. (2009) Shaping nano-/micro-particles for enhanced vascular interaction in laminar flows. *Nanotechnology 20*, 495101.
(44) Arnida, Janát-Amsbury, M. M., Ray, A., Peterson, C. M., and Ghandehari, H. (2011) Geometry and surface characteristics of gold nanoparticles influence their biodistribution and uptake by macrophages. *Eur. J. Pharm. Biopharm. 77*, 417−23.
(45) Bruckman, M., Jiang, K., Simpson, E. J., Randolph, L. N., Luyt, L. G., Yu, X., and Steinmetz, N. F. (2014) Dual-modal magnetic resonance and fluorescence imaging of atherosclerotic plaques in vivo using VCAM-1 targeted tobacco mosaic virus. *Nano Lett. 14*, 1551−8.
(46) Ms, B., Farkas, M. E., Aanei, I. L., Behrens, C. R., Tong, G. J., Murphy, S. T., Neil, J. P. O., and Francis, M. B. (2013) PET imaging and biodistribution of chemically modified bacteriophage MS2. *Mol. Pharmaceutics 10*, 69−76.
(47) Zeng, Q., Wen, H., Wen, Q., Chen, X., Wang, Y., Xuan, W., Liang, J., and Wan, S. (2013) Cucumber mosaic virus as drug delivery vehicle for doxorubicin. *Biomaterials 34*, 4632−42.
(48) Abourbeh, G., Shir, A., Mishani, E., Ogris, M., Rödl, W., Wagner, E., and Levitzki, A. (2012) PolyIC GE11 polyplex inhibits EGFR-overexpressing tumors. *IUBMB Life 64*, 324−30.
(49) Tang, H., Chen, X., Rui, M., Sun, W., Chen, J., Peng, J., and Xu, Y. (2014) Effects of surface displayed targeting ligand GE11 on liposome distribution and extravasation in tumor. *Mol. Pharmaceutics 11*, 3242−3250.
(50) Song, S., Liu, D., Peng, J., Sun, Y., Li, Z., Gu, J.-R., and Xu, Y. (2008) Peptide ligand-mediated liposome distribution and targeting to EGFR expressing tumor in vivo. *Int. J. Pharm. 363*, 155−61.
(51) Pokorski, J. K., Hovlid, M. L., and Finn, M. G. (2011) Cell targeting with hybrid Qβ virus-like particles displaying epidermal growth factor. *ChemBioChem 12*, 2441−7.
(52) Paraskevakou, G., Allen, C., Nakamura, T., Zollman, P., James, C. D., Peng, K. W., Schroeder, M., Russell, S. J., and Galanis, E. (2007) Epidermal Growth Factor Receptor (EGFR)− Retargeted Measles Virus Strains Effectively Target EGFR- or EGFRvIII Expressing Gliomas. *Mol. Ther. 15*, 677−686.

DOI: 10.1021/bc500545z
Bioconjugate Chem. 2015, 26, 262−269